

# Measurement and prediction of CTOD in austenitic stainless steel

W. Khor <sup>a,b</sup>, P.L. Moore <sup>c</sup>, H.G. Pisarski <sup>c</sup>, M. Haslett <sup>c</sup>, C.J. Brown <sup>a, †</sup>

<sup>a</sup> Brunel University London, Uxbridge, UB8 3PH

<sup>b</sup> NSIRC, Granta Park, CB21 6AL

<sup>c</sup> TWI, Granta Park, CB21 6AL

† Author to receive correspondence: [chris.brown@brunel.ac.uk](mailto:chris.brown@brunel.ac.uk)

## Abstract

Variation of Crack Tip Opening Displacement (CTOD) test values can have a significant effect on the Engineering Critical Assessment of a structure. This paper examines the development of CTOD with increasing load in an austenitic stainless steel.

The silicone replication method giving variation of CTOD across the specimen thickness, and Digital Image Correlation (DIC) are compared to each other, and in turn to clip gauge measurements from tests. Results from Finite Element models are also presented.

Estimations of CTOD from BS 7448-1, ISO 12135 and ASTM E1820, and a proposed modification from JWES are compared to the experimental data from the crack cast in silicone compound – assumed to be the actual CTOD.

The DIC measurement showed consistency with crack replicas, and a formula is given to estimate CTOD using DIC. For high strain hardening austenitic stainless steel, both the JWES and ASTM E1820 estimations provide adequate accuracy for CTOD.

## Nomenclature

$A_p$  = plastic area under  $P$  vs.  $V_p$

$a_0$  = initial crack length

$B$  = specimen thickness

$B_0$  = remaining ligament,  $W - a_0$

$b$  = position on section as a ratio of  $B/2$

$E$  = modulus of elasticity

$J$  = strain energy around the crack

$K$  = stress intensity factor

$K_I$  = stress intensity factor in mode I loading

$m$  = plane strain function used in JWES

$m_{ASTM}$  = function relating  $J$  to CTOD

$n$  = strain hardening exponent

$P$  = load

$r_p$  = rotational factor for plastic hinge assumption

$V_g$  = clip gauge opening displacement

$V_p$  = plastic component of clip gauge opening displacement

$W$  = specimen width

$z$  = knife edge height

$\delta$  = crack tip opening displacement (CTOD)

$\delta_5$  = direct CTOD measurement from two points at the specimen surface 5mm apart, placed directly at the crack tip

$\delta_{5\text{ DIC}}$  =  $\delta_5$  measured using the DIC technique

$\delta_{SRC}$  = CTOD measured on the silicone replicas

$\delta_{FE}$  = CTOD obtained from the FE model

$\nu$  = Poisson's ratio

$\sigma_{ys}$  = 0.2% proof strength at test temperature

$\sigma_{uts}$  = ultimate tensile strength at test temperature

$\sigma_y$  = flow stress at test temperature,  $(\sigma_{ys} + \sigma_{uts})/2$

$\varepsilon$  = strain

$\eta$  = geometrical based calibration function for  $J$

## Introduction

Fracture toughness is used in Engineering Critical Assessment (ECA) to assess the fitness-for-service of engineering structures with respect to avoidance of fracture.<sup>1-5</sup> Differences in the values of fracture toughness measurements on the same specimen using different methods could result in a structure being considered safe or not. It is therefore important that the estimation of failure criteria, such as critical flaw size, does not result in over-conservative design, while still ensuring structural integrity.<sup>6</sup>

Crack Tip Opening Displacement (CTOD) is a measure of the physical opening of an original crack tip in a standard fracture toughness test specimen at the point of stable or unstable crack extension. The CTOD concept was proposed by Wells<sup>7</sup> using notched tension bars. In the early days, a 'COD meter' had been used to measure CTOD.<sup>8</sup> It was placed at the bottom of a sawn notch and the opening of the crack could be measured directly. Modern techniques introduce a fatigue pre-crack in fracture toughness specimens to mimic an actual crack. Displacement data is obtained by measuring the displacement of the load or the opening of the crack mouth (CMOD) from which CTOD is inferred.<sup>9,10</sup>

Current standards-based procedures – such as BS 7448-1<sup>9</sup>, ISO 12135<sup>11</sup>, and ASTM E1820<sup>10</sup> - specify methods to determine fracture toughness, including determination of the critical CTOD for the material under the application of slowly increasing loading on the specimen. The fracture test procedure and methodology is well established and is similar between standards. A clip gauge is often used to measure the displacement data from the opening of the crack mouth due to its consistency<sup>12</sup> and simplicity. However, despite the similar testing methods, different standards give different CTOD estimation equations<sup>13</sup>. Figure 1a shows an SENB specimen with the clip gauge attached prior to testing, while Figure 1b shows the same specimen after testing.

BS 7448-1 and ISO 12135 use the same equation for CTOD based on the assumption of the development of a plastic hinge, while ASTM E1820 calculates CTOD based on a different fracture toughness parameter,  $J$ .<sup>14-16</sup>  $J$  is defined as the path-independent strain energy around the crack.<sup>17</sup> Recently, researchers at the Japanese Welding Engineering Society (JWES) have suggested a modification to include a strain hardening consideration in the calculation used in BS 7448-1.<sup>18</sup>

A potential application for the JWES strain hardening modification can occur when stainless steel is used. Austenitic stainless steel is often used in harsh environments due to its corrosion resistance properties.<sup>19-22</sup> When compared to typical structural and high strength steel, austenitic stainless steel can have significantly higher strain hardening, which is a result of its

high ductility. This ductility usually implies better fracture toughness properties, which in turn leads to reduced engineering safety concerns, but it is still important that this design criterion is assessed. Grade 300 austenitic stainless steel typically contains 18% Chromium, 10% Nickel and 1% Manganese with the balance being made up by Iron.<sup>23</sup>

The current study was carried out to examine the validity of the available standard equations when applied to austenitic stainless steel. In a standard Single Edge Notched Bend (SENB) test, the crack width was estimated using standard clip gauges. Silicone casting and Digital Image Correlation (DIC) were used to measure CTOD directly, and a Finite Element (FE) model was used to simulate the experimental results. The CTOD measurements were not limited to low CTOD values.

## Material and methods

Experiments were carried out using standard SENB testing procedures, in accordance with BS 7448-1 (Fig 1). SS316 plate was used as the austenitic stainless steel for experimental testing. Mechanical and chemical properties are given in Tables 1 and 2 respectively. Strain hardening,  $n$ , was estimated by fitting an offset power law equation to the tensile data obtained from a standard tensile test. 21mm thick plate was machined to nine standard  $B \times 2B$  SENB specimens, where  $B = 20\text{mm}$ . All SENB specimens are fatigue pre-cracked to a nominal initial crack length of  $a_0/W = 0.5$ . A full list of all the tests carried out is given in Table 3.

### Physical crack casting

Physical crack measurement has been a challenge. It is clear from others<sup>24</sup> that a section can be sectioned to measure CTOD – with the consequence that only one measurement per specimen may be made. More recently Tagawa *et al.*<sup>13</sup> and Kawabata *et al.*<sup>18</sup> have used the silicone compound method to replicate the physical crack. However the castings were limited to one per specimen and confined to  $\text{CTOD} \leq 0.2\text{mm}$ . A more extensive process is described here.

One of the  $B \times 2B$  SENB specimens, labelled M03-05 was used for the physical crack replication test. The crack replication test was similar to a standard test, except that the specimen was held at constant displacement at chosen loads, while a 2-part silicone compound (Microset RF-101) was used to make a cast of the crack (Fig 2a). After the silicone compound had cured (approximately 5 minutes for each casting), the specimen was further loaded and held at the next chosen load (Fig 2b), when it was possible to remove the cured crack replica (Fig 2c), and the casting procedure was then repeated.

## Image measurements

Image measurements are becoming more viable to measure crack development. The  $\delta_5$  method was first devised in the 1980's in Germany.<sup>25</sup>  $\delta_5$  is the displacement between two fixed measurement points set initially 5mm apart on the specimen surface at both sides of the crack tip. For a standard  $\delta_5$  test, a special instrument called a  $\delta_5$  clip is used to measure the CTOD directly, and the displacement is recorded as the increasing loading is applied. Others adopted the technique and report initial work on thin specimens.<sup>26</sup> More recently Ktari *et al.*<sup>27</sup> have used Digital Image Correlation (DIC) effectively for crack opening measurement.

DIC measurement was applied on seven different fracture toughness specimens (M03-11 to M03-17), which were tested in a single point SENB setup. A commercial non-contact optical 3D deformation measuring system, GOM-ARAMIS v6.3, was used during these tests to determine  $\delta_5$ .

By using GOM-ARAMIS, the software is able to recognize the surface structure of the measured object in digital camera images and allocates coordinates to the image pixels. Hence, instead of using  $\delta_5$  clips, two stage points with a distance of 5mm can be defined directly on the recorded images, the displacements of the two points can be obtained from the recorded series of testing images, and  $\delta_5$  can be calculated throughout the test. Fig 3 shows the two points recognized on the surface of the specimen for  $\delta_5$  measurement, and the displacement of the respective points after the specimen is loaded. The  $\delta_5$  is considered to give an alternative estimation of crack displacement to the CTOD values determined from the standard tests. It provides a direct measurement of CTOD at the surface which may differ from CTOD within the interior of the specimen.

Austenitic stainless steels exhibit high strain hardening and are capable of large plastic deformation. In a three-point-bend test, it was found that the displacement measuring clip gauge often achieved its limit mid-test and required adjustment to continue measurement. DIC, however, measures displacement based on the speckle patterns it recognises on the surface, which can provide continuous surface displacement measurement.

## Finite element models

The FE method has often been applied to investigate fracture toughness estimation equations.<sup>13,18,24,28-30</sup> A Geometrically and Materially Non-linear Analysis (GMNA) FE model was used to predict CTOD in an SENB setup. A fully three-dimensional quarter SENB model was simulated using commercially available software (ABAQUS v6.14) with a blunted crack tip of 0.03mm radius. The blunted crack tip allows better deformation of the crack tip at larger deformation level. Symmetry was defined on the x-y plane on the side of the specimen facing

in the z-direction and the y-z plane on the unbroken ligament facing the x-direction. Fig 4 shows the outline geometry of the SENB specimen investigated and the detail of the mesh adjacent to the crack. Both 8-noded elements (C3D8R) and 20-noded elements (C3D20R) were used to model the SENB specimen. The 20-noded elements gave a better representation of the actual specimen and thus were used in the subsequent sections.

A modulus of elasticity of 200 GPa and Poisson's ratio of 0.3 was used to define the elastic properties, and the experimentally determined true stress-strain properties used for post-elastic material definition are shown in Fig 5. Displacement in the negative y-direction was applied on the upper roller, whereas the lower roller was fixed. 104736 elements were generated for the model and a standard convergence test was performed based on varying the element size distributed across the crack tip. CTOD was measured based on opening of the original crack tip.

## Results

The CTOD measured on the Silicone Replica Crack (SRC) was considered as representative of the actual physical crack at the particular loading, and used to compare against the other CTOD measurements, finite element predictions, and CTOD estimation equations. In order to compare experimental and FE results, the lower clip gauge opening is converted to CMOD using Equation 1, which is derived from ASTM E1290.<sup>31</sup>

$$CMOD = \frac{V_g}{1 + \frac{z}{0.8a_0 + 0.2W}} \quad \text{Eq.1}$$

## Experimental CTOD measurements

Once removed, the silicone replicas were sliced at  $b = -0.5, 0, \text{ and } 0.5$ , giving five sections across the replica (Fig 6). CTOD was then measured on the sliced crack replicas using an optical microscope (Fig 7). The values of CTOD obtained from the silicone replicas are plotted in Fig 8 for increasing loads, represented by increasing CMOD.

The specimen was ductile and experienced large deformation in the test. A significant crack tip deformation before tearing, known as the stretch zone was expected. However the stretch zone width was included in the measurement of original crack length,  $a_0$ , due to difficulties in isolating the start and end of the stretch zone width accurately under the microscope. Hence it might be expected that the CTOD measured on the silicone replicas could be fractionally smaller than the actual CTOD.

The load-displacement plot (Fig 9) for the crack replication test shows load reductions at loads where the crack is replicated by insertion of silicone. This phenomenon is due to load relaxation when the specimen is held at constant displacement.<sup>32</sup> However this phenomenon

does not appear to have any significant effect on the overall load-displacement plot and differences between this and a standard test, also shown in Fig 9 are negligible. The non-linear nature of CMOD with increasing load can be observed.

## DIC method for surface measurement

Seven specimens (M03-11 to M03-17) were tested in the SENB configuration. Compiling  $\delta_{5DIC}$  measurements for each of the seven specimens at loads 10.0 kN, 15.0 kN, 20.0 kN, 25.0 kN and 27.5 kN, and comparing to the clip gauge readings taken at the same load, it was found (Fig 10) that the  $\delta_{5DIC}$  measurements were highly correlated to their equivalent clip gauge displacement data ( $R^2= 0.9970$ ).

## Finite Element CTOD measurements

The load-displacement relation obtained from the FE model is also shown in Fig 9. From the FE model, CTOD was determined at three points across the section,  $b= 0$  (centre), 0.5, and  $b=1$  (edge). Due to symmetry of the model, these points would also correspond to  $b= 0, -0.5,$  and  $-1$  in a complete model. Fig 11 shows the relation between CTOD and CMOD, both determined from the FE model. Fig 9 has shown the close agreement between measured and FE modelled CMOD up to a value of about 5 mm; discrepancies that occur after 5 mm are discussed further below.

## Discussion

The CTOD estimation equations used in the standards (BS 7448-1, ISO 12135 and JWES) were based on research which did not cover material with high strain hardening properties.<sup>33</sup> <sup>34</sup> Fig 12 shows CTOD measured from the SRC specimens at the centre ( $b=0$ ), and the average of the two edge values ( $b=\pm 1$ ), plotted against the value measured using DIC for austenitic stainless steel. The measurements at the surface are both the same estimate of CTOD, and it can be seen that very good agreement is obtained using a linear relation<sup>35</sup> with  $R^2= 0.9974$ . DIC measurements might be more conservative than the surface CTOD from SRC at large displacement. This is because the measurements are taken at an offset rather than directly at the crack tip (Fig 13).<sup>36</sup> However, this not thought to be a problem here.

From Fig 6 it can be seen that the line defining the crack tip front is curved. The straight crack front FE model (Fig 11) shows that the CTOD is greater at the crack centre than at the outside surfaces but Fig 12 shows that the value of  $\delta_{SRC}$  at the sides is greater than that at the centre. However, from Fig 14 it can be seen that the geometry and the assumption of a constant point

of specimen rotation dictates otherwise, and the curved crack front means a lower value of  $\delta_{SRC}$  is found at the centre.

A consistent relationship between  $\delta_{5\ DIC}$  and  $\delta_{SRC (b=0)}$  is observed (Fig 12) for  $\delta_{5\ DIC} > 0.5\text{mm}$ , indicating a little-changing difference between the crack width at the centre of the specimen and that at the outer edges. CTOD at the centre of the specimen is approximately 0.34mm lower than at the surface CTOD for the crack front curvature present in this specimen. Eq.2 shows the relation of  $\delta_{5\ DIC}$  to  $\delta_{SRC (b=0)}$ .

$$\delta_{SRC (b=0)} = 1.0716\delta_{5\ DIC} - 0.3827 \quad \text{Eq.2}$$

The elastic CTOD equations in BS 7448-1, ASTM E1820 and in the JWES equation assume plane strain conditions for the estimation of CTOD. By investigating the strain data across the crack tip obtained from the FE model, it is found that conditions approximating plane strain are achieved across much of the thickness. CTOD at  $b=0$  is considered the 'plane strain' CTOD estimated by the standardized equations; this is discussed further later in the paper.

A straight crack front model was simulated in FE as an idealized test specimen. Pook has provided a useful retrospective<sup>37</sup> of the importance of 3-D effects on the crack front, and in particular, the importance of understanding the consequences of a curved crack front. A linear elastic analysis<sup>38</sup> show similarities between the FE and stress intensity factor models.

The measured initial crack length of the sides of the specimen tested is shorter than the initial crack length on the middle of the specimen. This phenomenon is a result of the fatigue loading on the specimen, which is used to induce a crack. Fig 11 shows the CTOD obtained at different positions across the crack front, which shows an opposite trend when compared to the CTOD measured from the silicone replicas in Fig 8. These findings are consistent with Hutchison & Pisarski's<sup>29</sup> FE predictions, where straight crack front models give larger CTOD in the middle of the crack front while a curved crack front model gives larger CTOD in the sides of the crack. Analysing the effect of crack length using the similar triangles principle used in BS 7448-1, a lower  $a_0/W$  ratio (shorter crack length) would result in higher CTOD, as described above for the experimental results.

The CTOD obtained from FE and standardized estimation equations were compared to that measured on the silicone replica (Fig 15). The FE model and BS 7448-1 overestimate the silicone replica CTOD for all values of CTOD, while ASTM E1820 and JWES overestimate low values of CTOD, but underestimate towards larger CTOD values. Experimentally, stable ductile tearing initiates under large deformation at the crack tip; in the FE model, the crack tip continues deforming under increasing load, as damage mechanisms and crack extension were not accounted for in the model. Fig 15 shows that the FE estimations become close to

the SRC measurements at larger CTOD values ( $\delta_{SRC (b=0)} > 1\text{mm}$ ). The larger difference observed in lower CTOD values in the FE model is due to the blunted crack tip used which might result in an increase in CTOD when compared to a fatigue pre-cracked notch.<sup>39</sup>

If an underestimation of CTOD up to 15% is considered acceptable, both the JWES equation and ASTM E1820 estimation can be considered to be acceptable predictors of  $\delta_{SRC(b=0)}$ . Based on CTOD measured in the  $\delta_{SRC (b=0)} > 1\text{mm}$  region, JWES gives a very good estimation of  $\delta_{SRC (b=0)}$ . In the range  $\delta_{SRC (b=0)} > 0.5\text{mm}$ , ASTM E1820 gives a lower value of CTOD, but generally within the 15% limit. The overestimation of the lower values of CTOD is due to the underestimation of the physical CTOD, a result of the inclusion of stretch zone width in the determination of the original crack length,  $a_0$ , resulting in the overestimation being more obvious in the lower CTOD region, e.g.  $\delta_{SRC (b=0)} < 0.5\text{mm}$ . The results suggest that the JWES and ASTM E1820 methods are better alternatives than BS 7448-1 to estimate CTOD in high strain hardening austenitic stainless steels.

Based on the results obtained from the silicone replicas and FE, it was found that the Japanese modification to the BS 7448-1 and ISO 12165 equation, and the ASTM E1820 estimation are both recommended for determining CTOD for austenitic stainless steel and high strain hardening materials. The JWES CTOD equation for SENB specimens is given by<sup>18</sup>

$$\delta = K^2 \frac{(1 - \nu^2)}{m\sigma_{ys}E} + f\left(B, \frac{\sigma_{ys}}{\sigma_{uts}}\right) \frac{0.43B_o V_p}{0.43B_o + a_0 + z}$$

where the correction factors are:-

$$m = 4.9 - 3.5 \left( \frac{\sigma_{ys}}{\sigma_{uts}} \right)$$

$$f(B) = 0.8 + 0.2 \exp\{-0.019(B - 25)\}$$

$$f\left(\frac{\sigma_{ys}}{\sigma_{uts}}\right) = -1.4 \left( \frac{\sigma_{ys}}{\sigma_{uts}} \right)^2 + 2.8 \frac{\sigma_{ys}}{\sigma_{uts}} - 0.35$$

## Conclusions

This paper has shown the measurement of CTOD using silicone replicas.  $\delta_5$  DIC measurements have been validated using the silicone replica CTOD data. An FE model has been used to generate predictions of the experimental data.

For austenitic stainless steel and high strain hardening materials, CTOD measured on the silicone replica suggest that JWES give good estimates of CTOD for  $\delta_{SRC (b=0)} > 1\text{mm}$ . The ASTM E1820 estimation is an alternative for measuring  $\delta_{SRC (b=0)} < 1\text{mm}$ .

For high strain hardening materials, direct measurement of  $\delta_5$  at the specimen surface using the DIC approach can estimate CTOD for  $0.5\text{mm} < \delta_5_{DIC}$  using Equation 2. This equation provides a good estimate of CTOD for research applications; however, the use of DIC would not necessarily be practical for commercial test houses.

## **Acknowledgements**

The authors wish to acknowledge the funding and facility provided by TWI and NSIRC for this work. The authors also wish to thank Philip Cossey and Dan Bloom for assistance in the crack replication tests, Mark Tinkler for the setup of the DIC equipment and Prof. Tetsuya Tagawa for the updates and discussion on the silicone crack replication method.

## List of Figures

Fig 1a SENB specimen with double clip gauge attached before loading,

Fig 1b SENB specimen after loading without clip gauges

Fig 2a Crack casting process - filling the crack with silicone compound,

Fig 2b Crack casting process - specimen further loaded after silicone compound cures,

Fig 2c Crack casting process - cured crack replica removed from the crack

Fig 3 Determination of (a)  $\delta_5$  points based on (b) speckle pattern

Fig 4 Quarter SENB model showing boundary conditions, crack shape and mesh near the crack tip

Fig 5 True stress-strain properties used in the FE model

Fig 6 Silicone crack replica from M03-05, taken at  $CMOD = 2.031\text{mm}$ , showing the five equally spaced cross-sections for CTOD measurement, described in terms of  $b$ , where  $b=0$  is the middle of the specimen.

Fig 7 Definition of CTOD measured on the silicone replica ( $CMOD = 2.771\text{mm}$ ,  $b = 0$ )

Fig 8 CTOD at different position across thickness for different  $CMOD$  (selected points for clarity)

Fig 9 Load-displacement data obtained from the experiment and FE model

Fig 10 Clip gauge opening vs.  $\delta_5$  measured on the SS316 SENB specimens tested using DIC

Fig 11  $CMOD$  vs. CTOD at  $b = 0, 0.5$  and  $1$  obtained from the FE model

Fig 12 Comparison between  $\delta_5$  DIC,  $\delta$  SRC ( $b=0$ ) (plane strain CTOD), and  $\delta$  SRC ( $b=\pm 1$ ) (surface CTOD)

Fig 13 Geometrical analysis of  $\delta$  and  $\delta_5$  on (a) an idealized initial crack and (b) an idealized blunted crack

Fig 14 The effect of curved crack front on the determination of CTOD at the middle and side of the specimen

Fig 15 Comparison of the silicone replica CTOD,  $\delta$  SRC ( $b=0$ ) to FE CTOD,  $\delta$  FE ( $b=0$ ) and standard CTOD estimations

## List of Tables

Table 1 Tensile properties tested in accordance to BS EN ISO 6892-1:2009 B

Table 2 Chemical composition of SS316 by weigh percentage, measured using electrical discharge method

Table 3 Specimen numbering and description

## References

1. Shen G, Gianetto JA, Bouchard R, Bowker JT, Tyson WR (2004) Fracture Toughness Testing of Pipeline Girth Welds. *International Pipeline Conference*. Minister of Natural Resources, Canada, Calgary.
2. Gordon JR, Keith G, Gordon NC (2013) Defect and Strain Tolerance of Girth Welds in High Strength Pipelines. *International Seminar on Welding High Strength Pipeline Steels*. CBMM and TMS, USA, 365-394.
3. Sarzosa DFB, Souza RF, Ruggieri C (2015) J–CTOD relations in clamped SE(T) fracture specimens including 3-D stationary and growth analysis. *Engineering Fracture Mechanics*.
4. BSI (2014) BS 7910:2013 - Guide to methods for assessing the acceptability of flaws in metallic structures. BSI.
5. API (2007) API 579- Fitness-For-Service.
6. Anderson TL, Osage DA (2000) API 579: a comprehensive fitness-for-service guide. *International Journal of Pressure Vessels and Piping*. **77**: 953-963.
7. Wells AA (1969) Crack opening displacements from elastic-plastic analyses of externally notched tension bars. *Engineering Fracture Mechanics*. **1**: 399-410.
8. Burdekin FM, Stone DEW (1966) The crack opening displacement approach to fracture mechanics in yielding materials. *The Journal of Strain Analysis for Engineering Design*. **1**: 145-153.
9. BSI (1991) BS 7448-1:1991 - Fracture mechanics toughness tests — Part 1: Method for determination of  $K_{Ic}$ , critical CTOD and critical J values of metallic materials. BSI.
10. ASTM (2014) ASTM E1820-13 - Standard Measurement of Fracture Toughness. ASTM, 1-54.
11. ISO (2002) ISO 12135 - 02 Metallic materials - Unified method of test for the determination of quasistatic fracture toughness. ISO.
12. Kirk MT, Dodds Jr. RH (1993) J and CTOD Estimation Equations for Shallow Cracks in Single Edge Notch Bend Specimens. *Journal of Testing and Evaluation*. **21**: 228-238.
13. Tagawa T, Kawabata T, Sakimoto T, et al. (2014) Experimental measurements of deformed crack tips in different yield-to-tensile ratio steels. *Engineering Fracture Mechanics*. **128**: 157-170.

14. Shih CF (1981) Relationships between the J-integral and the crack opening displacement for stationary and extending cracks. *Journal of the Mechanics and Physics of Solids*. **29**: 305-326.
15. Kumar V, German MD, Shih CF (1981) An Engineering Approach for Elastic-Plastic Fracture Analysis. General Electric Company.
16. Zhu X-K, Joyce JA (2012) Review of fracture toughness (G, K, J, CTOD, CTOA) testing and standardization. *Engineering Fracture Mechanics*. **85**: 1-46.
17. Rice JR (1968) A Path Independent Integral and the Approximate Analysis of Strain Concentration by Notches and Cracks. *Journal of Applied Mechanics*. **35**: 379-386.
18. Kawabata T, Tagawa T, Sakimoto T, et al. (2016) Proposal for a new CTOD calculation formula. *Engineering Fracture Mechanics*. **159**: 16-34.
19. Ebara R (2002) Long-term corrosion fatigue behaviour of structural materials. *Fatigue and Fracture of Engineering Materials and Structures*. **25**: 855-859.
20. Spindler MW (2004) The multiaxial creep ductility of austenitic stainless steels. *Fatigue and Fracture of Engineering Materials and Structures*. **27**: 273-281.
21. Colin J, Fatemi A (2010) Variable amplitude cyclic deformation and fatigue behaviour of stainless steel 304L including step, periodic, and random loadings. *Fatigue and Fracture of Engineering Materials and Structures*. **33**: 205-220.
22. Rahimi S, Marrow TJ (2012) Effects of orientation, stress and exposure time on short intergranular stress corrosion crack behaviour in sensitised type 304 austenitic stainless steel. *Fatigue and Fracture of Engineering Materials and Structures*. **35**: 359-373.
23. ASTM (2006) ASTM A276-06 - Standard Specification for Stainless Steel Bars and Shapes. ASTM, 1-7.
24. Wang Y-Y, Reemsnyder HS, Kirk MT (1997) Inference Equations for Fracture Toughness Testing: Numerical analysis and Experimental verification. *ASTM STP 1321*. 469-484.
25. Schwalbe K-h (1995) Introduction of  $\delta_5$  as an Operational Definition of the CTOD and its Practical Use. *ASTM STP 1256*. 763-778.
26. Ipina JEP (1997) CTOD with slow stable crack growth: analysis of the elastic component. *Fatigue and Fracture of Engineering Materials and Structures*. **20**: 1075-1082.

27. Ktari A, Baccar M, Shah M, Haddar N, Ayedi HF, Rezai-Aria F (2014) A crack propagation criterion based on  $\Delta$ CTOD measured with 2D-digital image correlation technique. *Fatigue and Fracture of Engineering Materials and Structures*. **37**: 682-694.
28. Tagawa T, Kawabata T, Sakimoto T, et al. (2014) A New CTOD Calculation Formula, Considering Strain-hardening Property. *Procedia Materials Science*. **3**: 772-777.
29. Hutchison E, Pisarski HG (2013) Effects of Crack Front Curvature on J and CTOD determination in Fracture Toughness Specimens by FEA. *Proceedings of the ASME 2013 32nd International Conference on Ocean, Offshore and Arctic Engineering OMAE 2013*, Nantes, France.
30. Hutchison E, London T (2015) Simulation of Stable Ductile Tearing using Re-Mesh Techniques coupled with Nodal release incorporating constraint. *NAFEMS World Congress 2015*, San Diego, USA.
31. ASTM (2008) ASTM E 1290-08 - Standard Test Method for Crack-Tip Opening Displacement ( CTOD ) Fracture Toughness Measurement. ASTM, 1-15.
32. Tagawa T, Haramishi Y, Minami F (2011) Stress Relaxation Behavior of Low Carbon Structural Steels. *Quarterly Journal of the Japan Welding Society*. **29**: 48-54.
33. Lin IH, Anderson TL, Derit R, Dawes MG, DeWit R, Dawes MG (1982) Displacements and rotational ractors in Single Edge Notched Bend specimens. *International Journal of Fracture*. **20**: R3-R7.
34. Wu S-X (1983) Plastic rotational factor and J-COD relationship of three point bend specimen. *Engineering Fracture Mechanics*. **18**: 83-95.
35. Microsoft (2010) Microsoft Excel.
36. Verstraete MA, Denys RM, Van Minnebruggen K, Hertelé S, De Waele W (2013) Determination of CTOD resistance curves in side-grooved Single-Edge Notched Tensile specimens using full field deformation measurements. *Engineering Fracture Mechanics*. **110**: 12-22.
37. Pook LP (2013) A 50-year retrospective review of three-dimensional effects at cracks and sharp notches. *Fatigue and Fracture of Engineering Materials and Structures*. **36**: 699-723.

38. Pook LP (2000) Finite element analysis of corner point displacements and stress intensity factors for narrow notches in square sheets and plates. *Fatigue and Fracture of Engineering Materials and Structures*. **23**: 979-992.
39. Spink GM, Worthington PJ, Heald PT (1973) The Effect of Notch Acuity on Fracture Toughness Testing. *Materials Science and Engineering*. **11**: 113-117.

## Tables

**Table 1 Tensile properties tested in accordance to BS EN ISO 6892-1:2009 B**

Material	SS316
strain hardening, $n^1$	0.53
Plate thickness, mm	21
Yield to tensile ratio, $\sigma_{ys}/\sigma_{uts}$	0.48
0.2% offset proof strength, MPa	285.5
Tensile strength, MPa	595.3
Elongation, %	67.5

---

<sup>1</sup> Strain hardening measurement is based on curve fitting using offset power law equation

**Table 2 Chemical composition of SS316 by weigh percentage, measured using electrical discharge method**

<b>C</b>	<b>Si</b>	<b>Mn</b>	<b>P</b>	<b>S</b>	<b>Cr</b>	<b>Mo</b>	<b>Ni</b>	<b>Al</b>	<b>As</b>
0.021	0.26	1.76	0.037	0.003	17.4	1.94	10.1	<0.01	<0.01

<b>B</b>	<b>Co</b>	<b>Cu</b>	<b>Nb</b>	<b>Pb</b>	<b>Sn</b>	<b>Ti</b>	<b>V</b>	<b>W</b>	<b>Ca</b>
<0.001	0.19	0.37	<0.01	<0.002	0.01	<0.005	0.06	0.07	<0.001

**Table 3 Specimen numbering and description**

<b>Specimen Number</b>	<b>Description</b>	<b>Setup</b>
<b>M03-03</b>	Single point SENB test	nominally 20mmx40mm Bx2B SENB specimen
<b>M03-05</b>	Interrupted SENB test with silicone crack replication	
<b>M03-11</b>	Single point SENB test with DIC measurement	
<b>M03-12</b>		
<b>M03-13</b>		
<b>M03-14</b>		
<b>M03-15</b>		
<b>M03-16</b>		
<b>M03-17</b>		

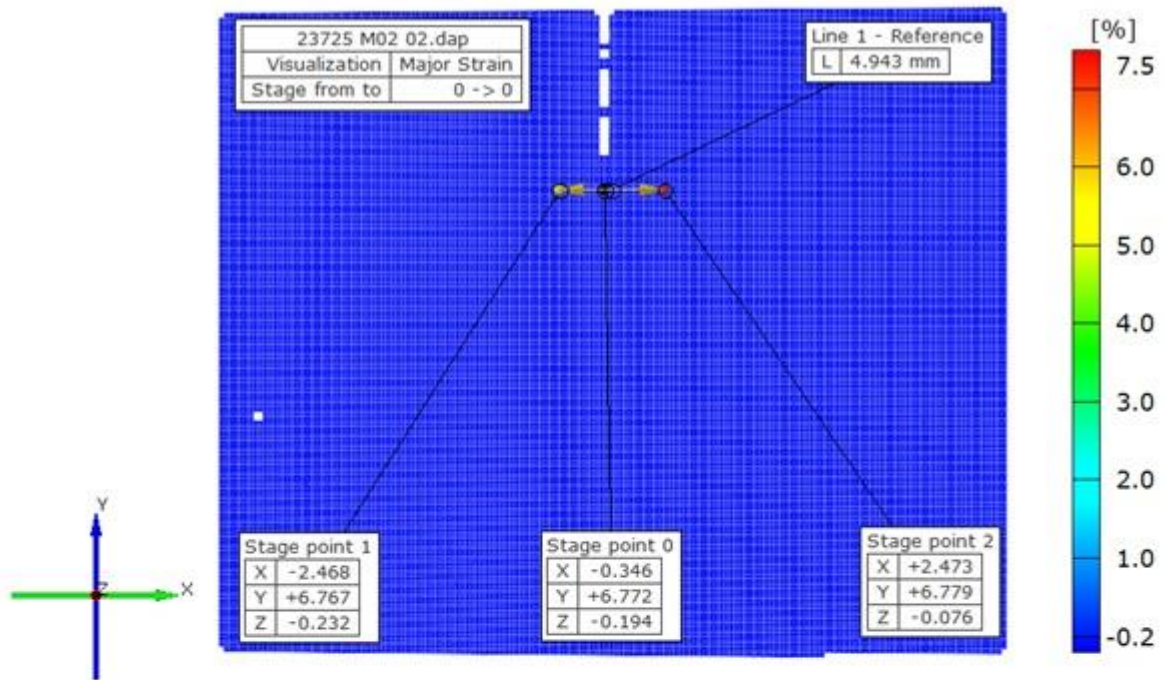




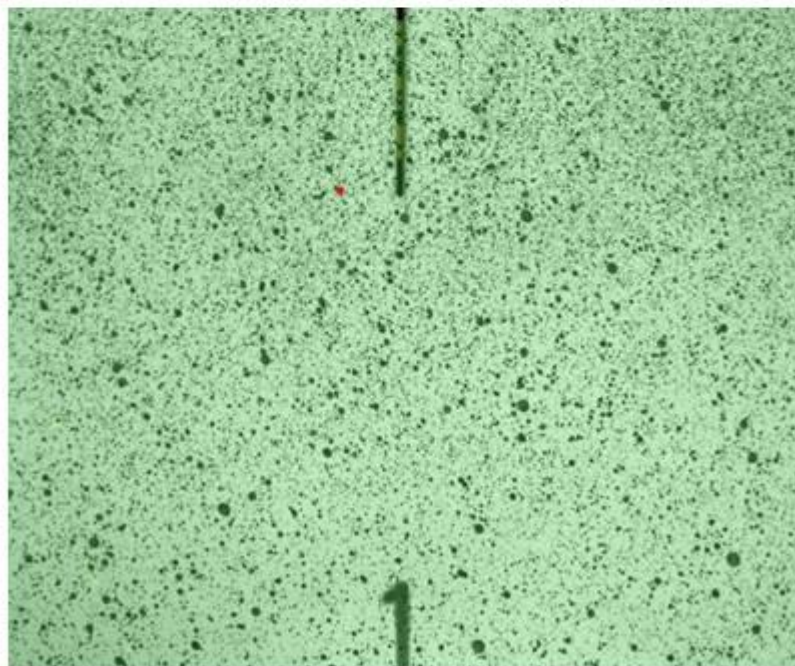




Z+



(a)



(b)

